URSI GASS 2020, Rome, Italy, 29 August - 5 September 2020

TeraFET Optimization for 100 GHz to 10 THz Operation

Xueqing Liu[(1)], Trond Ytterdal*[(2)], and Michael Shur[(1)]
(1) Department of Electrical, Computer, and Systems Engineering, Rensselaer Polytechnic Institute, Troy, NY 12180, USA
(2) Department of Electronic Systems, Norwegian University of Science and Technology, 7491 Trondheim, Norway

Abstract

We optimize the THz response for Si MOS TeraFET feature sizes from 10 nm to 300 nm in the 0.1 THz to 10 THz frequency range using both the analytical THz detector model and the compact multi-segment THz SPICE models. The models include the ballistic transport which is especially crucial for short channel devices in high THz frequencies. When the load resistance and series resistances are considered, the THz SPICE model should be used for more accurate results rather than the analytical model.

1 Introduction

TeraFET plasmonic technology enabled efficient detectors of terahertz (THz) and sub-THz radiation using Si MOS [1, 2], AlGaN/GaN HEMTs [3, 4], and AlGaAs/InGaAs HEMTs [5, 6]. TeraFETs could also be used as homodyne [7, 8] or heterodyne [9, 10] detectors, ratchet detectors [11], transceivers [12, 13], frequency multipliers [14, 15], or even as THz spectrometers/interferometers [16]. Other materials systems, such as p-diamond [17], have potential for developing efficient sub-THz detectors for possible Beyond 5G Wi-Fi applications. The analytical theory developed in [18, 19] and compact SPICE models [20, 21] have been used for simulation of TeraFETs. However, these investigations do not yield proposed optimized TeraFET design for specific sub-THz and THz bands covering the entire 100 GHz to 10 THz range. As shown in this paper, such optimization requires to account for the ballistic transport or quasi-ballistic transport, loading effects, and parasitic series resistances. Two other key optimization parameters are the TeraFET gate length and the operating regime (the gate bias). Our results show that optimizing the TeraFET design for a specific THz band could make orders of magnitude difference in the detector response.

The analytical model [18, 19] provides an excellent insight in the TeraFET physics, but it does not account for the loading effect and series resistances. These issues are fully accounted for by our multi-segment THz SPICE model based on the unified charge control model (UCCM) [20, 21].

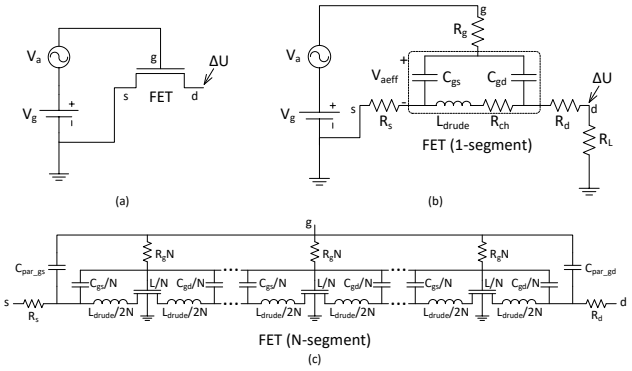

Figure 1. Equivalent circuit for the TeraFET detector (a) with open drain boundary condition and without series resistance and (b) with load and series resistances, and (c) multi-segment TeraFET SPICE model including series resistances and parasitic capacitances.

2 THz analytical and SPICE model

The analytical THz response was initially derived with assuming a small THz signal applied between the gate and the source and an open drain boundary condition [18]. Fig. 1 (a) shows such configuration for the analytical model, which gives the THz drain-to-source DC voltage response ΔU to the THz radiation inducing the voltage $V_a \cos \omega t$ between the gate and source

$$\Delta U = \frac{V_a^2}{4V_{gt}} f(\omega), \tag{1}$$

where $V_{gt} = V_{gs} - V_T$ is the gate voltage swing, V_T is the threshold voltage, $f(\omega) = 1 + \beta - \frac{1+\beta\cos(2k_o^{'}L)}{\sinh^2(k_o^{''}L)+\cos^2(k_o^{'}L)}$, $\beta = 2\omega\tau/(1+\omega^2\tau^2)^{1/2}$, $k_o^{'} = \frac{\omega}{s}[\frac{(1+\omega^{-2}\tau^{-2})^{1/2}+1}{2}]^{1/2}$, $k_o^{''} = \frac{\omega}{s}[\frac{(1+\omega^{-2}\tau^{-2})^{1/2}-1}{2}]^{1/2}$, $s = s_o[(1+\exp(-\frac{V_{gt}}{V_{th}}))\ln(1+\exp(\frac{V_{gt}}{V_{th}}))]^{1/2}$, $s_o = (\frac{qV_{th}}{m})^{1/2}$, $V_{th} = \frac{\eta k_B T}{q}$, q is the electric charge, k_B is the Boltzmann constant, T is temperature, η is the sub-threshold ideality factor, m is the electron effective mass.

To account for the series resistances at each terminal and the load resistance, the equivalent circuit used in the THz multi segment compact model [20, 21] is modified as Fig. 1 (b), where the intrinsic FET could be modelled by the channel resistance R_{ch}, Drude inductance L_{drude}, gate-to-source

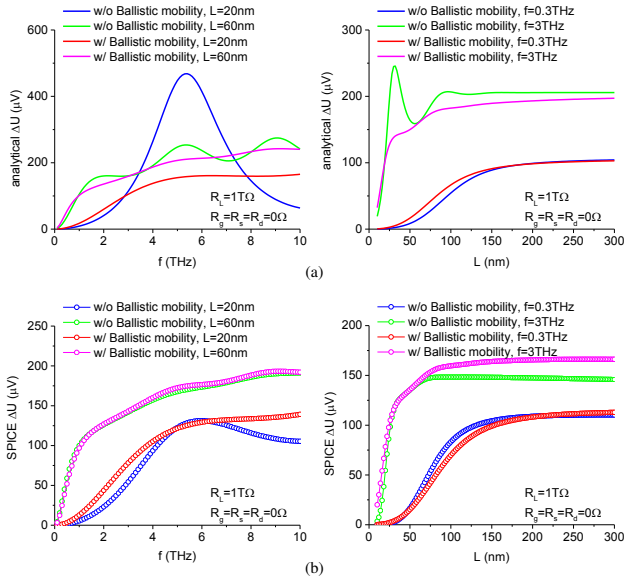

Figure 2. Effects of the ballistic transport on the THz response as functions of the signal frequency and channel length for (a) analytical model and (b) SPICE model. $V_{gt} = 0.21$ V and $V_a = 10$ mV. 50-segment SPICE model is used.

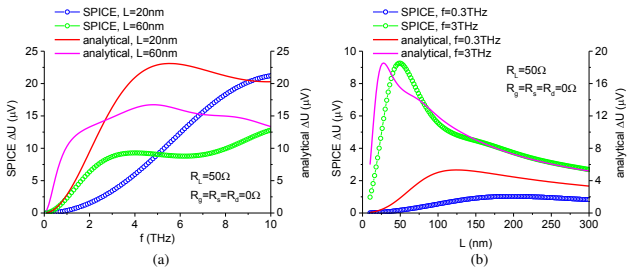

Figure 3. Comparison of the simulated and analytical THz response as a function of (a) THz signal frequency and (b) device channel length for $R_L = 50\,\Omega$ without series resistances. $V_{gt} = 0.21$ V and $V_a = 10$ mV. 50-segment SPICE model is used. Ballistic mobility is included.

capacitance C_{gs} and gate-to-drain capacitance C_{gd}. The equations for R_{ch}, C_{gs} and C_{gd} are described in the UCCM model [22]. The Drude inductance, $L_{drude} = \tau R_{ch}$, where $\tau = m\mu/q$ is the electron momentum relaxation time and μ is the mobility, accounts for the electron inertia effect which is important for the plasmonic resonant detection [23]. The modified analytical response could be estimated as

$$\Delta U = \frac{V_{aeff}^2}{4V_{gte}} f(\omega) \frac{1}{1+|Z_{ch}+R_s+R_d|/R_L}, \qquad (2)$$

where $V_{gte} = V_{th}[1+V_{gt}/(2V_{th}) + \sqrt{\delta^2 + (V_{gt}/(2V_{th})-1)^2}]$ is the effective gate voltage swing accounting for both above and below threshold, δ is a transition parameter between the above and below threshold, $V_{aeff} = |V_a - I_g R_g - I_s R_s|$ is the effective THz voltage applied on the intrinsic FET, $I_g = V_a/(R_g + Z_3 + \frac{(Z_1+R_s)(Z_2+R_d+R_L)}{Z_1+R_s+Z_2+R_d+R_L})$, $I_s = (V_a - I_g(R_g+Z_3))/(Z_1+R_s)$, $Z_t = Z_{sc} + Z_{dc} + Z_{ch}$, $Z_1 = Z_{ch}Z_{sc}/Z_t$, $Z_2 = Z_{ch}Z_{dc}/Z_t$, $Z_3 = Z_{sc}Z_{dc}/Z_t$, $Z_{ch} = R_{ch} + j\omega L_{drude}$, $Z_{sc} = 1/(j\omega C_{gs})$, $Z_{dc} = 1/(j\omega C_{gd})$. For more accurate determination of the THz response, it is desirable to use the THz SPICE model with the intrinsic FET split into multiple segments and including series resistances and parasitic capacitances [20, 21], as shown in Fig. 1 (c).

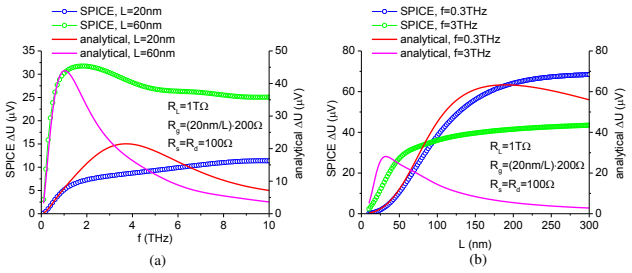

Figure 4. Comparison of the simulated and analytical THz response as a function of (a) THz signal frequency and (b) device channel length for $R_L = 1\,\mathrm{T}\Omega$ with series resistances. $V_{gt} = 0.21$ V and $V_a = 10$ mV. 50-segment SPICE model is used. Ballistic mobility is included.

For submicrometer devices, the ballistic transport becomes very important and should also be included in the model [24]. The mobility μ considering the ballistic transport could be given by $1/\mu = 1/\mu_0 + 1/\mu_{bal}$, where μ_0 is the mobility without considering the ballistic transport, $\mu_{bal} = \alpha q L/(mv)$, $v = \min(v_F, v_{th})$, the constant α, thermal velocity v_{th} and Fermi velocity v_F are described in [25].

Using the modified analytical THz response expression (2) and the multi-segment SPICE model (50 segments), we first examine the effects of the ballistic transport on the THz response without considering the load resistance and series resistances. Fig. 2 shows the THz response as functions of the signal frequency and the channel length for both the analytical and SPICE models, where the load resistance is set as $1\,\mathrm{T}\Omega$ representing the open drain boundary condition. It could be seen that the ballistic mobility plays a more important role at high THz frequencies for short channel devices, while the SPICE model is affected less than the analytical model. Without the ballistic mobility, the SPICE simulation predicts a much smaller response than the analytical model especially at the resonant peaks. However, the frequency corresponding to the maximum signal and the shapes of the computed and analytical dependences are quite similar for the open circuit boundary conditions. Therefore, the analytical theory is still useful for the TeraFET optimization for the open circuit conditions, especially with the ballistic transport included.

The effects of the load resistance and series resistances on the THz response for the analytical and SPICE models are shown in Fig. 3 and Fig. 4, respectively. Here we use realistic values for the series resistances based on 20 nm FDSOI and consider the gate length dependence for the gate resistance. The results show much larger disagreement between the analytical model and the SPICE model when a finite load resistance or realistic series resistances are applied.

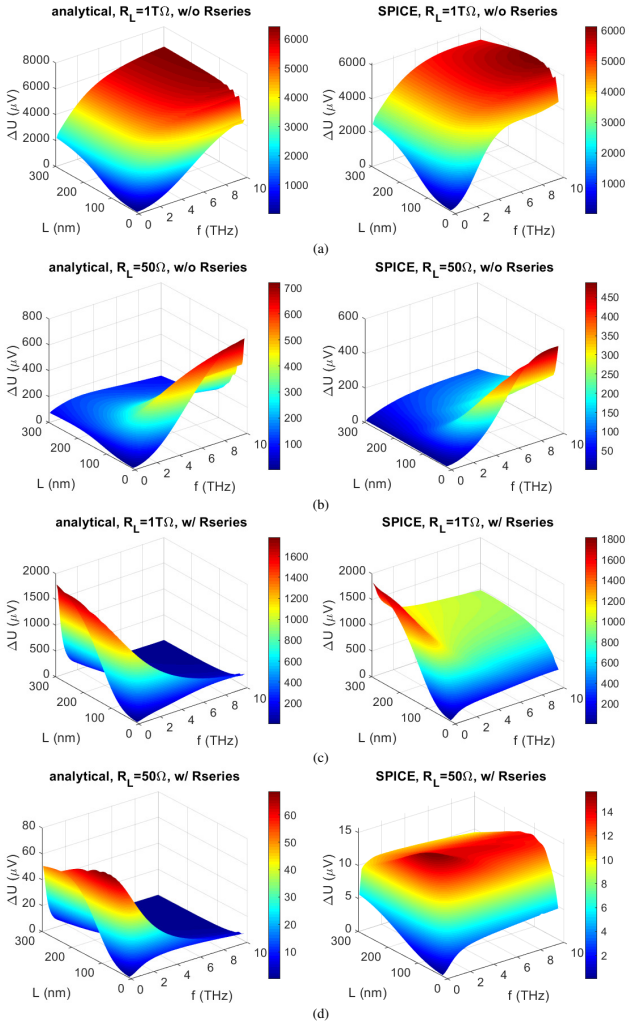

Figure 5. Analytical and simulated THz response as functions of signal frequency and channel length for (a) $R_L = 1\,\mathrm{T\Omega}$ and $R_g = R_s = R_d = 0\,\Omega$, (b) $R_L = 50\,\Omega$ and $R_g = R_s = R_d = 0\,\Omega$, (c) $R_L = 1\,\mathrm{T\Omega}$ and $R_g = (20\,\mathrm{nm/L})\cdot 200\,\Omega$ and $R_s = R_d = 100\,\Omega$, and (d) $R_L = 50\,\Omega$ and $R_g = (20\,\mathrm{nm/L})\cdot 200\,\Omega$ and $R_s = R_d = 100\,\Omega$. $V_{gt} = 0.21\,\mathrm{V}$ and $V_a = 50\,\mathrm{mV}$. 50-segment SPICE model is used. Ballistic mobility is included.

The reason could be due to the change of the boundary conditions or the different forms of the channel density in the UCCM equations and the analytical THz model. Equation (2) for the modified analytical THz response still includes the original function $f(\omega)$ which was derived with assuming the open drain boundary condition. Therefore, it could not accurately describe the analytical response accounting for a finite load resistance. Additionally, $f(\omega)$ assumes the channel density $n = CU/q$, while the UCCM gives a more complicated dependence of the channel density on the gate voltage. The effects of the series resistance on the channel density may not be included in the analytical model. Therefore, the THz SPICE model should give more accurate results than the analytical model when the loading and resistance effects are considered.

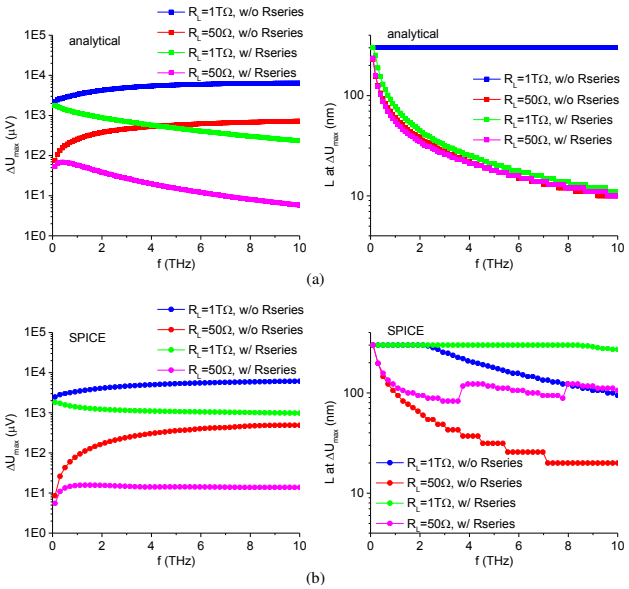

Figure 6. Maximum THz response and the corresponding channel length for (a) analytical model and (b) THz SPICE model from 0.1 THz to 10 THz. $V_{gt} = 0.21\,\mathrm{V}$ and $V_a = 50\,\mathrm{mV}$. $R_g = R_s = R_d = 0\,\Omega$ for w/o Rseries, while $R_g = (20\,\mathrm{nm/L})\cdot 200\,\Omega$ and $R_s = R_d = 100\,\Omega$ for w/ Rseries.

3 THz Response optimization

The analytical and SPICE models could be used for the THz response optimization, which is to find the maximum THz response within certain ranges of the signal frequency and channel length. For each frequency in the range from 0.1 THz to 10 THz, we first calculate or simulate the response from the analytical and SPICE models at each channel length from 10 nm to 300 nm. After we obtain the maximum response at a specific channel length, we could try the next frequency value and find the maximum response as well as the corresponding channel length in the whole frequency range. Fig. 5 shows the THz response as functions of the signal frequency and channel length for the analytical model. Fig. 6 shows the extracted maximum THz frequency and the corresponding feature size in the frequency range. The load resistance and series resistances could lead to very different optimization results. When these effects are considered, the rough estimation from the analytical model should be replaced by more accurate results from the THz SPICE model.

4 Conclusion

Using the modified analytical THz response model and the compact multi-segment THz SPICE model, we perform the THz response optimization for Si MOS TeraFET with feature sizes from 10 nm to 300 nm in the 0.1 THz to 10 THz frequency range. The ballistic transport is very important for short channel devices in high frequencies and should be included in the analytical and SPICE models. When the loading effects and series resistances are considered, the

THz SPICE model must be used for the device optimization. The obtained results could be used for Si TeraFET detector design in the 100 GHz to 10 THz range.

5 Acknowledgements

The work at RPI was supported by the U.S. Army Research Laboratory Cooperative Research Agreement (Project Monitor Dr. Meredith Reed) and by the US ONR (Project Monitor Dr. Paul Maki).

References

[1] W. Knap *et al.*, "Plasma wave detection of subterahertz and terahertz radiation by silicon field-effect transistors," *Appl. Phys. Lett.*, **85**, 4, July 2004, pp. 675–677.

[2] F. Teppe *et al.*, "Terahertz detectors based on plasma oscillations in nanometric silicon field effect transistors," *phys. stat. sol. (c)*, **2**, 4, March 2005, pp. 1413–1417.

[3] V. I. Gavrilenko *et al.*, "Electron transport and detection of terahertz radiation in a GaN/AlGaN submicrometer field-effect transistor," *Semiconductors*, **41**, 2, February 2007, pp. 232–234.

[4] A. El Fatimy *et al.*, "Terahertz detection by GaN/AlGaN transistors," *Electron. Lett.*, **42**, 23, November 2006, pp. 1342–1343.

[5] V. V. Popov *et al.*, "High-responsivity terahertz detection by on-chip InGaAs/GaAs field-effect-transistor array," *Appl. Phys. Lett.*, **98**, 15, April 2011, Art. No. 153504.

[6] W. Knap *et al.*, "Resonant detection of subterahertz radiation by plasma waves in a submicron field-effect transistor," *Appl. Phys. Lett.*, **80**, 18, May 2002, pp. 3433–3435.

[7] S. Preu *et al.*, "Terahertz detection by a homodyne field effect transistor multiplicative mixer," *IEEE Trans. Terahertz Sci. Technol.*, **2**, 3, May 2012, pp. 278–283.

[8] S. Rumyantsev *et al.*, "Homodyne phase sensitive terahertz spectrometer," *Appl. Phys. Lett.*, **111**, 12, September 2017, Art. No. 121105.

[9] D. Glaab *et al.*, "Terahertz heterodyne detection with silicon field-effect transistors," *Appl. Phys. Lett.*, **96**, 4, January 2010, Art. No. 042106.

[10] B. Gershgorin *et al.*, "Field effect transistor as heterodyne terahertz detector," *Electron. Lett.*, **44**, 17, August 2008, pp. 1036–1037.

[11] P. Faltermeier *et al.*, "Helicity sensitive terahertz radiation detection by dual-grating-gate high electron mobility transistors," *J. Appl. Phys.*, **118**, 8, August 2015, Art. No. 084301.

[12] S. Muralidharan, K. Wu, and M. Hella, "A 216GHz 0.5 mW transmitter with a compact power combiner in 65nm CMOS," in *Asia-Pac. Microwave Conf. (APMC)*, **2**, December 2015, pp. 1–3.

[13] K. Wu *et al.*, "A 220 GHz OOK Outphasing Transmitter in 130-nm BiCMOS Technology," in *IEEE BiCMOS and Compound Semicond. Integr. Circ. and Technol. Symp.*, October 2018, pp. 227–230.

[14] K. Wu, S. Muralidharan, and M. M. Hella, "A Wideband SiGe BiCMOS Frequency Doubler with 6.5-dBm Peak Output Power for Millimeter-Wave Signal Sources," *IEEE Trans. Microw. Theory Tech.*, **86**, 3, January 2018, pp. 187–200.

[15] S. Muralidharan, K. Wu, and M. Hella, "A 165-230GHz SiGe amplifier-doubler chain with 5dBm peak output power," in *IEEE Radio Freq. Integr. Circ. Symp. (RFIC)*, May 2016, pp. 302–305.

[16] I. V. Gorbenko, V. Y. Kachorovskii, and M. Shur, "Terahertz plasmonic detector controlled by phase asymmetry," *Opt. Express*, **27**, 4, February 2019, pp. 4004–4013.

[17] M. Shur *et al.*, "p-Diamond as candidate for plasmonic terahertz and far infrared applications," *Appl. Phys. Lett.*, **113**, 25, December 2018, Art. No. 253502.

[18] M. I. Dyakonov and M. S. Shur, "Detection, mixing, and frequency multiplication of terahertz radiation by two-dimensional electronic fluid," *IEEE Trans. Electron Devices*, **43**, 3, March 1996, pp. 380–387.

[19] M. I. Dyakonov and M. S. Shur, "Plasma wave electronics: novel terahertz devices using two-dimensional electron fluid," *IEEE Trans. Electron Devices*, **43**, 10, October 1996, pp. 1640–1645.

[20] X. Liu *et al.*, "Compact Terahertz SPICE Model: Effects of Drude Inductance and Leakage," *IEEE Trans. Electron Devices*, **65**, 12, December 2018, pp. 5350–5356.

[21] X. Liu *et al.*, "Compact terahertz SPICE/ADS model," *IEEE Trans. Electron Devices*, **66**, 6, April 2019, pp. 2496–2501.

[22] K. Lee, M. Shur, T. Fjeldly, and T. Ytterdal, *Semiconductor device modeling for VLSI*, Princeton, NJ, USA: Prentice Hall, 1993, pp. 441–478.

[23] M. Shur, "Plasma wave terahertz electronics," *Electron. Lett.*, **46**, 26, December 2010, pp. 18–21.

[24] M. Shur, "Ballistic transport and terahertz electronics," in *IEEE Int. Conf. Electron Devices Solid-State Circuits (EDSSC)*, December 2010, pp. 1-7.

[25] A. P. Dmitriev and M. S. Shur, "Ballistic admittance: Periodic variation with frequency," *Appl. Phys. Lett.*, **89**, 14, October 2006, Art. No. 142102.